Institutionen för systemteknik
Department of Electrical Engineering

Examensarbete

An iterative reconstruction algorithm for quantitative tissue decomposition using DECT

Examensarbete utfört i Datorseende
vid Tekniska högskolan vid Linköpings universitet
av

Oscar Grandell

LiTH-ISY-EX--12/4617--SE

Linköping 2012

Linköpings universitet
TEKNISKA HÖGSKOLAN

Department of Electrical Engineering
Linköpings universitet
SE-581 83 Linköping, Sweden

Linköpings tekniska högskola
Linköpings universitet
581 83 Linköping

Chapter 2

Theory

In this chapter the foundation theory upon which this thesis stands will be described. In Sections 2.1 to 2.6 the algorithms of computed tomography theory is described and in Section 2.11 the beam hardening artifact is presented. These sections are based on the work in [9], [10], and [11]. Finally in Sections 2.12 and 2.13 the three material decomposition and two material plus density decomposition will be described, which are based on the work in [1], [2], [3] and [12].

2.1 General projection generation

When generating projections, what is really calculated is line integrals through a 2D or 3D volume. By using the coordinate system in Fig. 2.1, an arbitrary line through the object, represented by a 2D function $f(x, y)$, can be described by

$$x\cos\theta + y\sin\theta = \rho. \tag{2.1}$$

A line integral can be calculated as

$$P_\theta(\rho) = \int\limits_{(\theta,\rho)\text{line}} f(x, y)ds. \tag{2.2}$$

By using a dirac delta function (2.2) can be rewritten as

$$P_\theta(\rho) = \int\limits_{-\infty}^{\infty}\int\limits_{-\infty}^{\infty} f(x, y)\delta(x\cos\theta + y\sin\theta - \rho)dxdy. \tag{2.3}$$

This is also known as the Radon transform. By combining a set of line integrals taken at different ρ but with constant θ, a projection is formed. The projections can be calculated using different settings, the simplest is collection of parallel rays known as parallel projections, Fig. 2.2a. A more common approach nowadays, especially in CT, is to use fan-beam projections, Fig. 2.2b. Here a single source sending out x-rays in a fan pattern is used, thus called fan-beam projections.

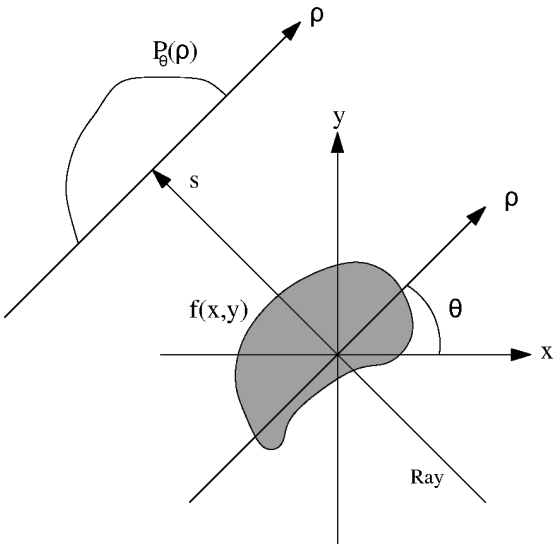

Figure 2.1: An object $f(x, y)$ and its projection $P_\theta(\rho)$ at angle θ.

2.2 Projection generation in CT

The projections generated by the CT scan is actually measurements of the attenuation of the material. In short a set of beams are sent through the object and an attenuation profile is measured on the other side. From the result obtained from this single projection there is no way of determining any major attributes of the scanned object, but by repeating from different angles and then projecting this measured attenuation profile over an empty image grid the object can be reconstructed. This technique is more commonly known as backprojection, which will be described in detail in Section 2.3.

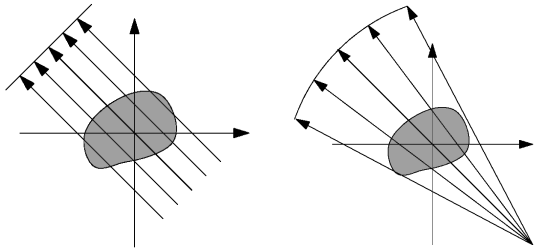

(a) Parallel. (b) Fan-beam.

Figure 2.2: Example of parallel and fan-beam generated projections.

2.2.1 Monochromatic projections

The beam attenuation in the material is mainly due to three different effects: the photoelectric effect, the Rayleigh scattering and the Compton scattering. The photoelectric absorption consists of a photon transferring all its energy to a tightly bound inner electron in an atom, while the Compton scattering is interaction between loosely bound or free electrons, making the photon change direction and loose some of its energy to the electron. The Rayleigh scattering is a function of the electric polarizability of the particles, and like the Compton scattering causes the photons to change direction.

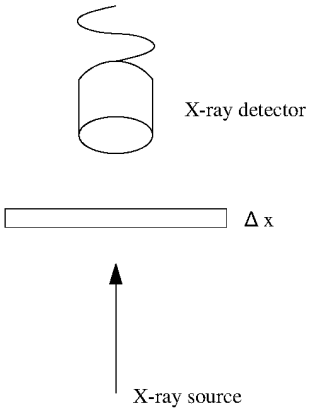

Figure 2.3: An x-ray tube sending out monochromatic photons through a thin slice of an unknown object.

Now consider the setup in Fig. 2.3, here N monochromatic photons travel through an unknown substance of width Δx and hit the detector. Due to the attenuation, $N - \Delta N$ will hit the detector. This can be described as in (2.4), where the attenuation coefficient μ is the probability per unit distance that the photon will be removed from the pencil beam, due to the combined effect of photoelectric absorption, Rayleigh and Compton scattering.

$$\frac{\Delta N}{N}\frac{1}{\Delta x} = -\mu \tag{2.4}$$

If Δx goes to zero in (2.4) a differential equation is obtained,

$$\frac{1}{N}dN = -\mu dx, \tag{2.5}$$

which can be solved as

$$\int_{N_0}^{N} \frac{1}{N}dN = -\mu \int_{0}^{x} dx \Rightarrow \ln\frac{N}{N_0} = -\mu x \Rightarrow N(x) = N_0 e^{-\mu x}, \tag{2.6}$$

where $N(x)$ is the number of photons at distance x. Here the assumption that μ is constant has been made, however is this not true most of the time. Instead consider Fig. 2.2, where a single x-ray beam travels in the s-direction through a function, $f(x, y)$, describing the attenuation of the material. It can then be described as

$$\int_{ray} \mu(x, y)ds = \ln\frac{N_s}{N_d}, \tag{2.7}$$

where N_s is the number of photons emitted from the source and N_d the number of photons detected.

2.2.2 Polychromatic projections

In the real world monochromatic x-ray sources are hard to find and x-ray spectra are used instead, see Fig. 2.4. Since the attenuation coefficient is dependent on the energy, (2.7) has to be rewritten to

$$N_d = \int S_{in}(E)e^{-\int \mu(x,y,E)ds}dE, \tag{2.8}$$

where $S_{in}(E)$ is the incident photon number density for energy level E.

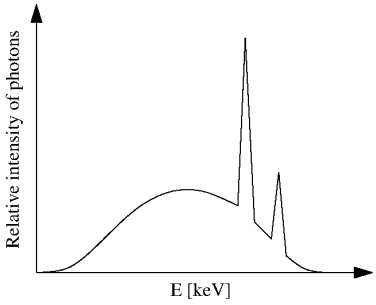

Figure 2.4: Example of a typical X-ray spectrum.

2.3 Backprojection

As mentioned in Section 2.2, the gathered data are smeared back over the image grid to reconstruct the object. This can mathematically be expressed as proposed in [10],

$$f_{\theta_k}(x, y) = P_{\theta_k}(\rho) = P_{\theta_k}(x\cos\theta_k + y\sin\theta_k), \tag{2.9}$$

where $f_{\theta_k}(x, y)$ is the result of backprojection at a certain angle, θ_k. Since this is true for all angles θ (2.9) can be rewritten as

$$f_\theta(x, y) = P_\theta(x\cos\theta + y\sin\theta). \tag{2.10}$$

The final image is then formed by integrating over all projection angles,

$$f(x,y) = \int_0^{2\pi} P_\theta(x\cos\theta + y\sin\theta)d\theta. \tag{2.11}$$

This will however result in a blurred image which is only an approximation of the true image.

2.4 The Fourier-Slice Theorem

The Fourier-slice theorem states the relationship between the 1D Fourier transform of a projection and the 2D Fourier transform of the region from which the projection was taken. The derivation here is similar to the one in [10]. This relation is the basis for reconstruction without blurring. The 1D Fourier transform of a projection can be written as

$$S_\theta(\omega) = \int_{-\infty}^{\infty} P_\theta(\rho)e^{-j2\pi\omega\rho}d\rho. \tag{2.12}$$

By inserting (2.3) in (2.12) the 1D Fourier transform can be written as

$$S_\theta(\omega) = \int_{-\infty}^{\infty}\int_{-\infty}^{\infty}\int_{-\infty}^{\infty} f(x,y)\delta(x\cos\theta + y\sin\theta - \rho)e^{-j2\pi\omega\rho}dxdyd\rho \tag{2.13}$$

$$= \int_{-\infty}^{\infty}\int_{-\infty}^{\infty} f(x,y)[\int_{-\infty}^{\infty} \delta(x\cos\theta + y\sin\theta - \rho)e^{-j2\pi\omega\rho}d\rho]dxdy \tag{2.14}$$

$$= \int_{-\infty}^{\infty}\int_{-\infty}^{\infty} f(x,y)e^{-j2\pi\omega(x\cos\theta + y\sin\theta)}dxdy, \tag{2.15}$$

and by using $u = \omega\cos\theta$ and $v = \omega\sin\theta$ the expression becomes

$$S_\theta(\omega) = [\int_{-\infty}^{\infty}\int_{-\infty}^{\infty} f(x,y)e^{-j2\pi(ux+vy)}dxdy]_{u=\omega\cos\theta;v=\omega\sin\theta}, \tag{2.16}$$

which is the 2D Fourier transform of $f(x,y)$. The Fourier-slice theorem can be summed up as in (2.17), which states that Fourier transform of a projection at a certain angle, θ, is located along a line at the same angle of the 2D Fourier transform of the region from which it was obtained, see also Fig. 2.5.

$$S_\theta(\omega) = [F(u,v)]_{u=\omega\cos\theta;v=\omega\sin\theta} = F(\omega\cos\theta, \omega\sin\theta) \tag{2.17}$$

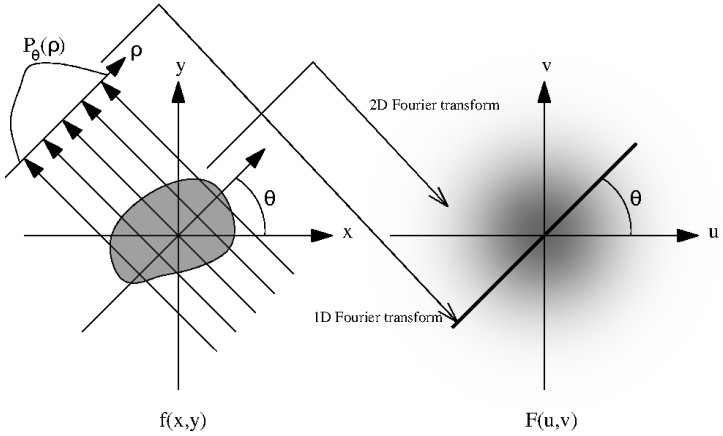

Figure 2.5: The Fourier slice theorem.

2.5 Filtered backprojection

Filtered backprojection is the most common way of reconstruction within computed tomography, but as stated in Section 2.3 normal backprojection only reconstructs the object approximately and a blurred image is obtained. One way to deal with this is to filter the projection data and use the properties of the Fourier slice theorem described in Section 2.4.

2.5.1 Parallel-beam filtered backprojection

Here follows a derivation of the filtered backprojection for a parallel-beam generated projection based on [11]. The object function $f(x, y)$ can be obtained by applying the inverse Fourier transform on the Fourier transform of the object,

$$f(x,y) = \int_{-\infty}^{\infty}\int_{-\infty}^{\infty} F(u,v)e^{j2\pi(ux+vy)}dudv. \tag{2.18}$$

A substitution from the rectangular coordinate system, (u, v), in the Fourier domain to a polar coordinate system, (ω, θ) via,

$$u = \omega\cos\theta, \quad v = \omega\sin\theta, \quad dudv = \omega d\omega d\theta, \tag{2.19}$$

gives the Fourier transform of a polar function as

$$f(x,y) = \int_{0}^{2\pi}\int_{0}^{\infty} F(\omega,\theta)e^{j2\pi\omega(x\cos\theta+y\sin\theta)}\omega d\omega d\theta. \tag{2.20}$$

The integral in (2.20) can be split into two by considering $0 \leq \theta < \pi$ and $\pi \leq \theta < 2\pi$ which gives

$$f(x,y) = \int_0^{\pi}\int_0^{\infty} F(\omega,\theta)e^{j2\pi\omega(x\cos\theta+y\sin\theta)}\omega d\omega d\theta + \int_0^{\pi}\int_0^{\infty} F(\omega,\theta+\pi)e^{j2\pi\omega[x\cos(\theta+\pi)+y\sin(\theta+\pi)]}\omega d\omega d\theta. \tag{2.21}$$

When using the Fourier property in (2.22) and combining it with (2.21), the expression in (2.23) is obtained.

$$F(\omega,\theta+\pi) = F(-\omega,\theta) \tag{2.22}$$

$$f(x,y) = \int_0^{\pi}\left[\int_{-\infty}^{\infty} F(\omega,\theta)|\omega|e^{j2\pi\omega(x\cos\theta+y\sin\theta)}d\omega\right]d\theta \tag{2.23}$$

The equation above can be simplified by setting $\rho = x\cos\theta + y\sin\theta$. The 2D Fourier transform $F(\omega,\theta)$ can be exchanged to the Fourier transform of the projection at angle θ, $S_\theta(\omega)$, to get

$$f(x,y) = \int_0^{\pi}\left[\int_{-\infty}^{\infty} S_\theta(\omega)|\omega|e^{j2\pi\omega\rho}d\omega\right]d\theta, \tag{2.24}$$

which also can be expressed as

$$f(x,y) = \int_0^{\pi} Q_\theta(\rho)d\theta = \int_0^{\pi} Q_\theta(x\cos\theta + y\sin\theta)d\theta, \tag{2.25}$$

where

$$Q_\theta(\rho) = \int_{-\infty}^{\infty} S_\theta(\omega)|\omega|e^{j2\pi\omega\rho}d\omega. \tag{2.26}$$

The last equation represents a filtering operation, where $|\omega|$ is a 1D filter in the Fourier domain called a ramp filter, and $Q_\theta(\rho)$ is the filtered projection. Equation (2.25) states that the object can be reconstructed by summation of all these filtered projections.

2.5.2 Fan-beam filtered backprojection

Nowadays not many parallel-beam CT scanners exist, this due to the fact the scan times become very long as the x-ray source has to linearly scan the object at all angles. Instead modern CT scanners use an x-ray point source that emits a fan-shaped beam, Fig. 2.2b, or even more modern using multiple fan-beams

at different pitch angles. These are referred to as multi-slice spiral CT or helical cone-beam scanners. As the beams no longer travel parallel to each other, the filtered backprojection has to be changed as well.
There are two types of fan-beam projections depending upon if the projections are sampled at equiangular or equispaced intervals. Here follows a derivation, similar as in [11], of how the filtered backprojection is altered in the case of equiangular rays.

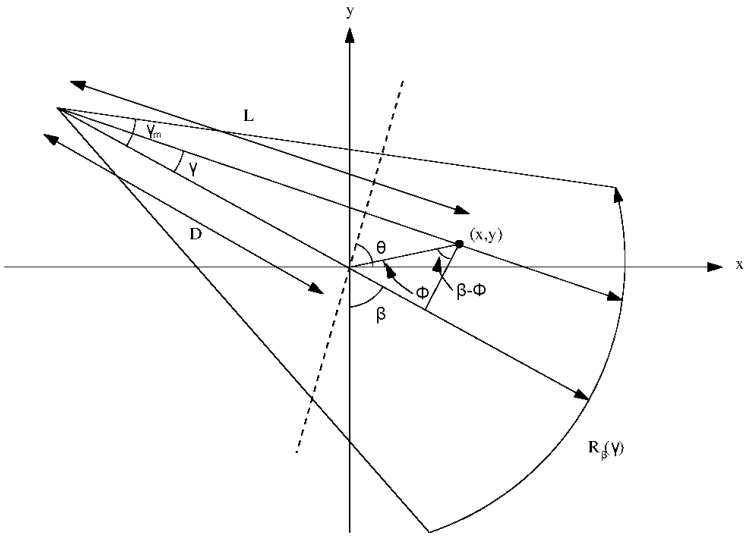

Figure 2.6: Equiangular geometry.

First consider the setup in Fig. 2.6 and let $R_\beta(\gamma)$ denote the projection obtained from a fan-beam. β is then the angle the source makes with a reference axis y, and the angle γ is the location of a ray within the fan in relation to the beam that hits the center of the detector. If the projection data would have been generated along a set of parallel rays and belonged to a parallel projection $P_\theta(\rho)$ it would have to satisfy the conditions

$$\theta = \beta + \gamma, \quad \rho = D \sin \gamma, \tag{2.27}$$

where D is the distance from the source to the origin. The object $f(x, y)$ can then be reconstructed as

$$f(x,y) = \int_0^\pi \int_{-\rho_m}^{\rho_m} P_\theta(\rho) h(x \cos\theta + y \sin\theta - \rho) d\rho d\theta, \tag{2.28}$$

where ρ_m is the value of ρ for which $P_\theta(\rho) = 0$ with $|\rho| > \rho_m$ in all projections. Equation (2.28) only requires parallel projections over an 180° interval, for reconstruction from fan-beam data, however, data from a 360° is necessary and the

equation has to be rewritten as

$$f(x,y) = \frac{1}{2}\int_0^{2\pi}\int_{-\rho_m}^{\rho_m} P_\theta(\rho)h(x\cos\theta + y\sin\theta - \rho)d\rho d\theta. \tag{2.29}$$

Derivation of the algorithm becomes easier when a point (x, y) is expressed in polar coordinates (r, ϕ) where

$$x = r\cos\phi, \quad y = r\sin\phi. \tag{2.30}$$

Then (2.29) can be written as

$$f(r,\phi) = \frac{1}{2}\int_0^{2\pi}\int_{-\rho_m}^{\rho_m} P_\theta(\rho)h(r\cos(\theta-\phi) - \rho)d\rho d\theta. \tag{2.31}$$

Using (2.27), this integral can be expressed in terms of β and γ as

$$f(r,\phi) = \frac{1}{2}\int_{-\gamma}^{2\pi-\gamma}\int_{-\sin^{-1}\rho_m/D}^{\sin^{-1}\rho_m/D} P_{\beta+\gamma}(D\sin\gamma)h(r\cos(\beta+\gamma-\phi)-D\sin\gamma)D\cos\gamma d\gamma d\beta. \tag{2.32}$$

Here a couple of observations can be made. Firstly the interval of $-\gamma$ to $2\pi - \gamma$ for β cover the entire 360° range that is needed, and since all functions of β are 2π-periodic the limits can be changed to 0 to 2π. The term $\sin^{-1}(\rho_m/D)$ is equal to the outermost ray that hits the detector, which is equal to γ_m so the limits can be replaced with $-\gamma_m$ to γ_m. Last, the expression $P_{\beta+\gamma}(D\sin\gamma)$ corresponds to a ray integral in the parallel projection data $P_\theta(\rho)$, and its correspondence in the fan-beam geometry is $R_\beta(\gamma)$. This results in that (2.32) can be rewritten as

$$f(r,\phi) = \frac{1}{2}\int_0^{2\pi}\int_{-\gamma_m}^{\gamma_m} R_\beta(\gamma)h(r\cos(\beta+\gamma-\phi) - D\sin\gamma)D\cos\gamma d\gamma d\beta. \tag{2.33}$$

This equation can be further simplified, for proof see [11], by using the following relations from Fig. 2.6

$$r\cos(\beta+\gamma-\phi) - D\sin\gamma = L\sin(\gamma'-\gamma), \tag{2.34}$$

where

$$\gamma' = \tan^{-1}\frac{r\cos(\beta-\phi)}{D + r\sin(\beta-\phi)}, \tag{2.35}$$

and

$$h(L\sin\gamma) = \left(\frac{\gamma}{L\sin\gamma}\right)^2 h(\gamma). \tag{2.36}$$

This allows (2.33) to be written as

$$f(r,\phi) = \int_0^{2\pi} \frac{1}{L^2} \int_{-\gamma_m}^{\gamma_m} R_\beta(\gamma) g(\gamma' - \gamma) D \cos\gamma d\gamma d\beta, \tag{2.37}$$

where

$$g(\gamma) = \frac{1}{2} \left(\frac{\gamma}{\sin\gamma} \right)^2 h(\gamma). \tag{2.38}$$

Equation (2.37) can be interpreted as a weighted filtered backprojection, since it can be written as

$$f(r,\phi) = \int_0^{2\pi} \frac{1}{L^2} Q_\beta(\gamma') d\beta, \tag{2.39}$$

where

$$Q_\beta(\gamma) = R'_\beta(\gamma) * g(\gamma), \tag{2.40}$$

and

$$R'_\beta(\gamma) = R_\beta(\gamma) D \cos\gamma. \tag{2.41}$$

2.6 Fan-beam to parallel-beam rebinning

Another approach is to transform the fan-beam data to parallel data, this process is also known as rebinning. Once the data has been rebinned we can use parallel filtered backprojection to reconstruct. This approach has a few advantages compared to the weighted fan-beam filtered backprojection, with the greatest being that it is not as computationally heavy as the fan-beam filtered backprojection. Also, the angular scanning interval can be reduced. Another advantage in this thesis is that the projection calculations in the iterative algorithm, see Section 3.2, becomes easier to calculate. Here follows a derivation of how the rebinning can be done, similar as in [11]. As was seen in Section 2.5.2 the relationship between fan-beam projections and parallel projections are given by (2.27), namely

$$\theta = \beta + \gamma, \quad \rho = D \sin\gamma, \tag{2.42}$$

or equivalently

$$\beta = \theta - \gamma, \quad \gamma = \sin^{-1}\left(\frac{\rho}{D}\right). \tag{2.43}$$

So by using interpolation and the relationship in (2.43) it is possible to rebin the fan-beam data to parallel data and use parallel filtered backprojection. Another observation to be made is that parallel projections that are 180° apart are mirror images of each other,

$$P_\theta(\rho) = P_{\theta+\pi}(-\rho). \tag{2.44}$$

This implies that to reconstruct the object, a fully 360° interval with the fan-beam projections is no longer necessary, only an interval that lets us rebin to a 180°

interval. The relation in (2.44) also implies that an object can be reconstructed as long as we have

$$\theta_0 \leq \theta < \theta_0 + \pi. \tag{2.45}$$

By extending this to the fan-beam case, two ray integrals represented by the fan-beam angles (β_1, γ_1) and (β_2, γ_2) are identical if

$$\beta_1 - \gamma_1 = \beta_2 - \gamma_2 + \pi, \tag{2.46}$$

where

$$\gamma_1 = -\gamma_2, \tag{2.47}$$

for full proof see [11]. This means that a scanning interval for the fan-beam of only 180° is not enough, the scan has to be over $180° + 2\gamma_m$ interval to be able to rebin to a 180° interval without losing data, Fig. 2.8 compared to Fig. 2.7. Here γ_m is the angle from the central detector element to the outermost element, see Fig. 2.6.

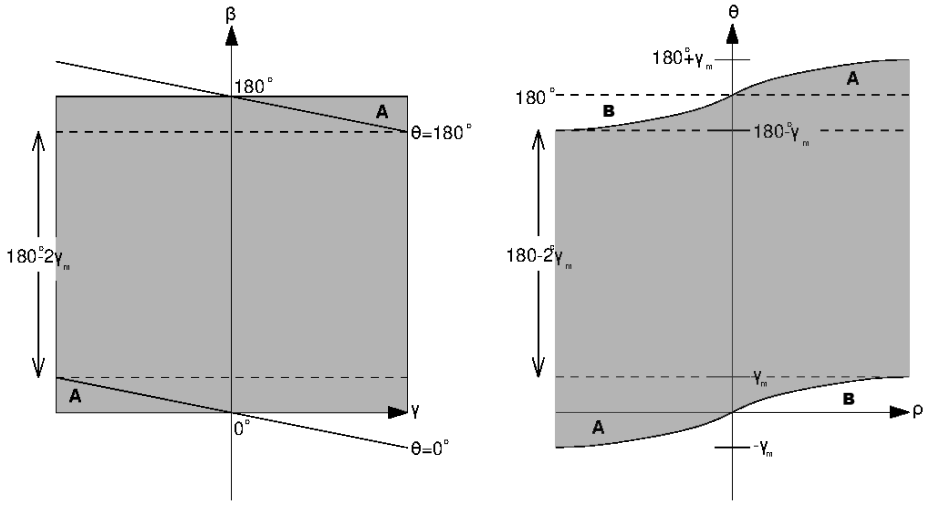

(a) Fan-beam data.

(b) Parallel data.

Figure 2.7: Rebinning of fan-beam data, shaded, to parallel with too few angles. The area A will be unnecessary when rebinned, and area B will be missing.

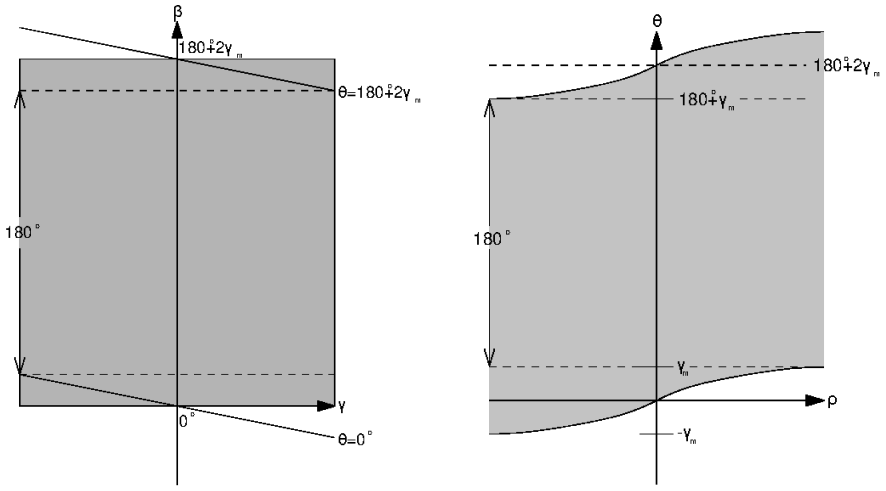

(a) Fan-beam data. (b) Parallel data.

Figure 2.8: Rebinning of fan-beam data, shaded, to parallel data. By scanning the extra $2\gamma_m$ a full 180° interval can be obtained.

2.7 Forward projection

In the iterative algorithm, see Section 3.2, both monochromatic and polychromatic projections are calculated. This can be done in different ways, a common way is to use Joseph's Method [13], which is presented here.
The method used by Joseph, assumes that the object function, $f(x, y)$, is slowly varying so that linear interpolation can be used between the pixels and that the image consists of $N \times N$ pixels in a Cartesian grid. Then consider an exactly straight ray K specified as

$$y(x) = -\cot(\theta) + y_0, \tag{2.48}$$

or

$$x(y) = -y\tan(\theta) + x_0, \tag{2.49}$$

where θ is the angle to the y-axis and y_0/x_0 is the cross-point with the y-axis/x-axis. The desired line integral $P(K)$ is dependent on whether the rays direction lies closer to the x or y axis and can be written as

$$P(K) = \begin{cases} \frac{1}{|\sin\theta|}\int f(x, y(x))dx & \text{for } |\sin\theta| \geq \frac{1}{\sqrt{2}} \\ \frac{1}{|\cos\theta|}\int f(x(y), y)dy & \text{for } |\cos\theta| \geq \frac{1}{\sqrt{2}} \end{cases}. \tag{2.50}$$

These can then be approximated by a Riemann sum and the x-direction integral becomes

$$P(K) = \frac{1}{|\sin\theta|}\left[\sum_{n=2}^{N-1} F_{n,n'} + \lambda_n(F_{n,n'+1} - F_{n,n'}) + T_1 + T_N\right], \tag{2.51}$$

where T_1 and T_N represents the first and last pixels along each ray, $F_{n,n'} = f(x_n, y_{n'})$ and λ_n is defined as

$$\lambda_n = y(x_n) - n', \quad n' = \text{integer part of } y(x_n), \tag{2.52}$$

by rewriting the inner part of (2.51)

$$F_{n,n'} + \lambda_n(F_{n,n'+1} - F_{n,n'}) = (1 - \lambda_n)F_{n,n'} + \lambda_n F_{n,n'+1}, \tag{2.53}$$

the linear interpolation becomes even more clear.

2.8 Monochromatic and polychromatic projections

The monoenergetic projection P_{mE} at effective energy E_1 for base material m with linear attenuation coefficient μ_{mE} can be calculated with Joseph's method which gives,

$$P_{mE_1} = \mu_{mE} l_m. \tag{2.54}$$

The polyenergetic projection is also calculated with Joseph's method, and by using,

$$P_{U_1} = \ln\left(\frac{S_{in}}{S_0}\right) = -\ln\left(\frac{S_0}{S_{in}}\right), \tag{2.55}$$

where S_{in} is the incident-photon intensity and S_0 is the exiting-photon intensity given by

$$S_{in} = \sum_{0}^{E_{max}} EN(E), \tag{2.56}$$

$$S_0 = \sum_{0}^{E_{max}} EN(E)e^{-\left(\sum_{m=1}^{M} \mu_m(E) l_m\right)} = \sum_{0}^{E_{max}} EN(E)e^{-\left(\sum_{m=1}^{M} \sigma_m(E)\rho_m l_m\right)}, \tag{2.57}$$

where E is the photon energy, $N(E)$ is the number of photons, $\mu_m(E)$ is the linear attenuation coefficient and ρ_m the density of material m and l_m is the length of intersection with material m calculated by using (2.54). Since $\mu_m(E) = \rho_m \sigma_m(E)$, where $\sigma_m(E)$ is the mass attenuation coefficient, the calculated density given by the decomposition methods 3MD or 2MD+ρ, Section 2.12 and 2.13, should be used instead of the predefined density of the pure material. This is especially necessary for bone decomposition with 2MD+ρ since the mixtures density is not linearly dependent on the components densities. For the 3MD method ρ is given by (2.71) and for the 2MD+ρ, ρ is given by

$$\rho = \frac{1}{\frac{w_1}{\rho_1} + \frac{w_2}{\rho_2}}. \tag{2.58}$$

2.10.2 Mixture of gaussians

Another method is to use the known correct values of the linear attenuation coefficients, $p_j = (\mu_{80}, \mu_{140})^T$, and assign each sample to the closest, in other words using a nearest neighbor approach. As seen in Fig. 2.10a the classification will with high probability fail. Instead the method can be further extended in a way

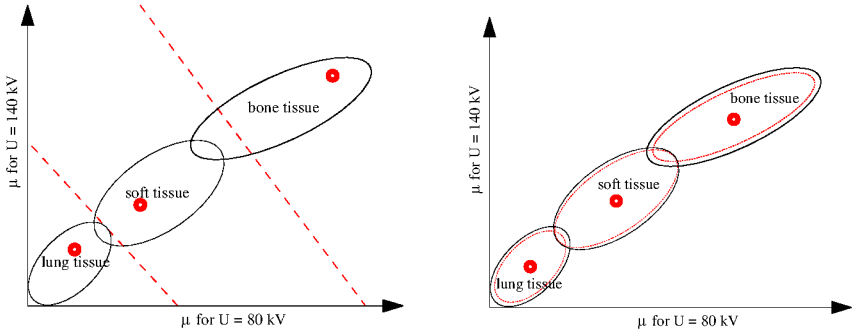

(a) Nearest neighbour method.

(b) Mixture of gaussians method.

Figure 2.10: Advanced methods for tissue segmentation.

that each correct value is also assigned a Gaussian covariance matrix, C_j. By using an iterative semi supervised training method the mean of all pixels assigned to each class and the convergence matrix adapts to the spreading of each class. This allows for using other parameters than the Euclidean distance. In fact we classify each pixel according to

$$\arg\max_j f(x_i; p_j, C_j) = \frac{1}{2\pi|C_j|^{\frac{1}{2}}} e^{-\frac{1}{2}(x_i - p_j)^T C_j^{-1}(x_i - p_j)}, \tag{2.59}$$

j here represent the class. This gives a result as Fig. 2.10b.

2.11 Beam hardening

The beam hardening artifact takes the shape of a cupping of the image or streaks in it. This is due to the interaction between the material and the x-rays, which occur in three different ways, coherent scattering or Raylight scattering, incoherent scattering or Compton scattering and the photoelectric effect. The linear attenuation coefficient, $\mu[m^{-1}]$, measured by the CT scanner can be described as a summation of these, i.e.

$$\mu(E) = \rho(\mu_{m_{Co}}(E) + \mu_{m_{In}}(E) + \mu_{m_{Ph}}(E)), \tag{2.60}$$

where $\rho[kg/m^3]$ is the density of the material and $\mu_m[m^2/kg]$ is the mass attenuation coefficient of the interaction process. A typical appearance of the linear attenuation coefficient with respect to the energy level is shown in Fig. 2.11.

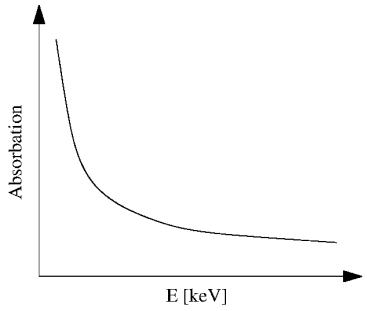

Figure 2.11: Example of an attenuation curve.

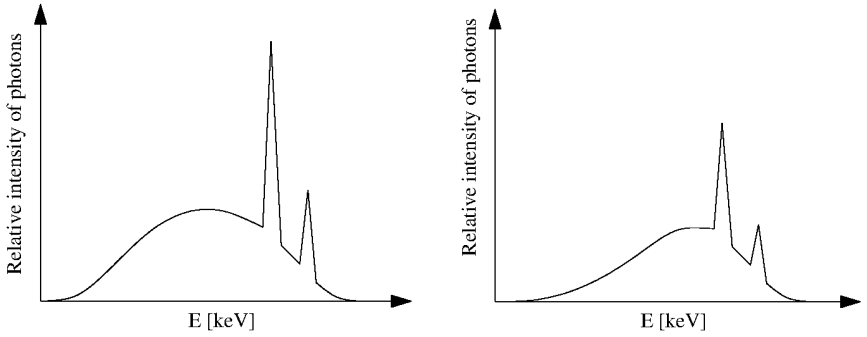

(a) Entering spectrum.

(b) Exiting spectrum.

Figure 2.12: Comparison between entering and exiting spectrum.

When a polychromatic beam in the form of an x-ray spectra, Fig. 2.12a, passes the object, the photons with lower energy has a higher probability of being absorbed, see Fig. 2.11 and [9]. This leads to the beam having a more narrow or harder spectra when exiting the object, Fig. 2.12b.

2.12 Three material decomposition

The three material decomposition method, 3MD, presented here is based on [1], [3] and [12].
Assume that a material is built up of three separate components, with mass attenuation coefficients $\frac{\mu_1}{\rho_1}$, $\frac{\mu_2}{\rho_2}$ and $\frac{\mu_3}{\rho_3}$ respectively. μ_i is the linear attenuation coefficient and ρ_i is the density. The law of mixtures can be applied on the mass attenuation coefficients if we assume that the mass is conserved, which is true in most cases. This is stated in (2.61) and (2.62).

$$\frac{\mu(E)}{\rho} = w_1\frac{\mu_1(E)}{\rho_1} + w_2\frac{\mu_2(E)}{\rho_2} + w_3\frac{\mu_3(E)}{\rho_3} \tag{2.61}$$

$$w_1 + w_2 + w_3 = 1 \tag{2.62}$$

Chapter 3

Methods

In this chapter a simple beam hardening correction algorithm and the iterative algorithm will be presented, as well as the modifications of them that had to be done. Last, the three phantoms that were used in the evaluation process are presented.

3.1 Simple water beam hardening correction

The simple water beam hardening correction, SWBHC, see for example [11], is based upon the fact that for a monochromatic beam the intensity of the exiting pencil beam can be calculated as (3.1), see Section 2.2.1,

$$S_{exit} = S_{in} e^{-\int \mu(E_0, l) dl}, \tag{3.1}$$

which in the case of a homogenous phantom (e.g. a water phantom) can be written as

$$S_{exit} = S_{in} e^{-\mu(E_0) l}, \tag{3.2}$$

while in the case of a polychromatic spectrum the relationship between the incident spectrum and exiting spectrum can be described as in (2.8),

$$S_{exit} = \int S_{in}(E) e^{-\int \mu(E, l) dl} dE. \tag{3.3}$$

However, for both cases the projection data for image reconstruction is calculated as

$$P_{mono} = -\ln\left(\frac{S_{exit}}{S_{in}}\right) \quad P_{poly} = -\ln\left(\frac{S_{exit}}{S_{in}}\right), \tag{3.4}$$

where

$$S_{in} = \int_0^{E_{max}} E S_{in}(E) dE. \tag{3.5}$$

For the monochromatic case this implies a linear relationship between the measured data and the linear attenuation coefficient, by combining (3.1) and (3.4), (3.6) is obtained,

$$P_{mono} = \ln\left(\frac{S_{in}}{S_{exit}}\right) = \mu(E_0)l. \tag{3.6}$$

For the polychromatic case however, this is not true, and a nonlinear relationship is obtained due to the beam hardening. This can be seen in Fig. 3.1, where the obtained projection data $\ln\left(\frac{S_{in}}{S_{exit}}\right)$ has been calculated at different thicknesses, l.

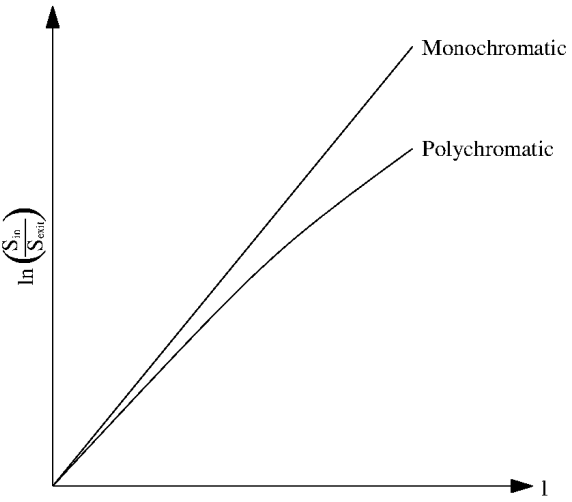

Figure 3.1: Projection data, $\ln\left(\frac{S_{in}}{S_{exit}}\right)$, for the monochromatic and polychromatic cases plotted against the thickness, l.

However, with the knowledge of this relationship a simple correction can be made. The approach is to via the polychromatic projection data find the width of the object, l_0, and with the use of it find the correct monochromatic projection value. First an effective linear attenuation coefficient is calculated as the energy-fluence weighted linear attenuation coefficient, for example according to [2], as

$$\mu_{mE} = \frac{\int_0^{E_{max}} EN(E)\mu(E)dE}{\int_0^{E_{max}} EN(E)dE}, \tag{3.7}$$

where E is the energy, $N(E)$ is the relative intensity of photons and $\mu(E)$ is the linear attenuation coefficient.
A normal way to present a CT scan is by Hounsfield numbers, these are calculated according to (3.8). In (3.8) μ_w is the effective linear attenuation coefficient for water and corresponds to μ_{mE} in (3.7).

$$HU = \frac{\mu - \mu_w}{\mu_w} \times 1000 \tag{3.8}$$

μ_{mE} is then used to compute the monochromatic projection curve $\mu_{mE}l$, see Fig. 3.2. Now the trick is to find the thickness, l, via the polychromatic curve. Once l is found the monochromatic projection value is calculated as

$$P_{mono} = \mu_{mE} l, \tag{3.9}$$

and a correction factor, c_{corr}, can be calculated as

$$c_{corr} = \frac{P_{mono}}{P_{poly}} = \frac{\mu_{mE} l}{\ln\left(\frac{S_{in}}{S_{exit}}\right)}. \tag{3.10}$$

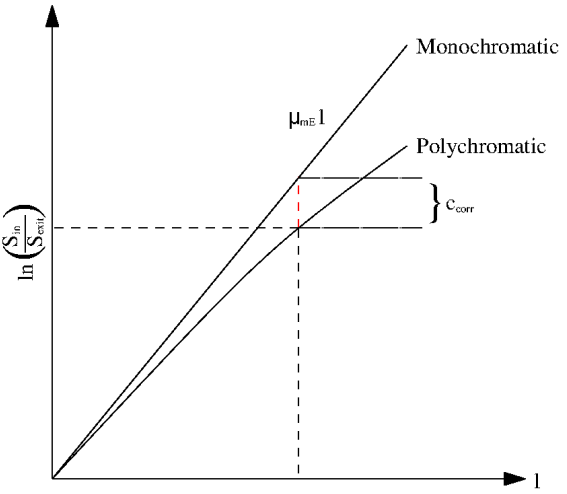

Figure 3.2: Graphical interpretation of the simple water beam hardening correction

The correction factor can then be used to correct the polychromatic projection by a simple multiplication,

$$P_{poly} c_{corr} = \ln\left(\frac{S_{in}}{S_{exit}}\right) \frac{\mu_{mE} l}{\ln\left(\frac{S_{in}}{S_{exit}}\right)} = \mu_{mE} l = P_{mono}. \tag{3.11}$$

This method works perfectly for a homogeneus substance and fairly well for objects containing similar tissues, for example other soft tissues. However, for bone tissue, which has different attenuation and density, the beam hardening will alter the numbers to much for it to correct them in a similar way as for the chosen material (e.g. water).